Article

Association between nanoscale strains and tissue level nanoindentation properties in age-related hip-fractures

Bonicelli, Andrea, Tay, Tabitha, Cobb, Justin P, Boughton, Oliver R, Hansen, Ulrich, Abel, Richard L and Zioupos, Peter
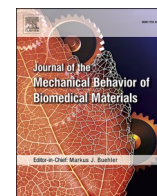
Association between nanoscale strains and tissue level nanoindentation properties in age-related hip-fractures

Andrea Bonicelli [a,b], Tabitha Tay [c], Justin P. Cobb [c], Oliver R. Boughton [c], Ulrich Hansen [d], Richard L. Abel [c], Peter Zioupos [b,*]

[a] School of Natural Sciences, University of Central Lancashire, Preston, PR1 2HE, UK
[b] Musculoskeletal & Medicolegal Research Group, Cranfield Forensic Institute, Defence Academy of the UK, Shrivenham, Swindon, SN6 8LA, UK
[c] MSk Laboratory, Department of Surgery and Cancer, Faculty of Medicine, Imperial College London, London, W6 8PR, UK
[d] The Biomechanics Group, Department of Mechanical Engineering, Faculty of Engineering, London, SW7 2AZ, Imperial College London, London, UK

A B S T R A C T

Measurement of the properties of bone as a material can happen in various length scales in its hierarchical and composite structure. The aim of this study was to test the tissue level properties of clinically-relevant human bone samples which were collected from donors belonging to three groups: ageing donors who suffered no fractures (Control); untreated fracture patients (Fx-Untreated) and patient who experienced hip fracture despite being treated with bisphosphonates (Fx-BisTreated). Tissue level properties were assessed by (a) nanoindentation and (b) synchrotron tensile tests (STT) where strains were measured at the 'tissue', 'fibril' and 'mineral' levels by using simultaneous Wide-angle - (WAXD) and Small angle- X-ray diffraction (SAXD). The composition was analysed by thermogravimetric analysis and material level endo- and exo-thermic reactions by differential scanning calorimetry (TGA/DSC3+). Irrespective of treatment fracture donors exhibited significantly lower tissue, fibril and mineral strain at the micro and nanoscale respectively and had a higher mineral content than controls. In nanoindentation only nanohardness was significantly greater for Controls and Fx-BisTreated versus Fx-Untreated. The other nanoindentation parameters did not vary significantly across the three groups. There was a highly significant positive correlation ($p < 0.001$) between organic content and tissue level strain behaviour. Overall hip-fractures were associated with lower STT nanostrains and it was behaviour measured by STT which proved to be a more effective approach for predicting fracture risk because evidently it was able to demonstrate the mechanical deficit for the bone tissue of the donors who had experienced fractures.

1. Introduction

Bone quality has recently emerged as a key factor in understanding the various age-related bone fragility fracture conditions. It is the amalgamation of physicochemical characteristics which give bone its material and structural properties at tissue level (Larrue et al., 2011; Seeman and Delmas, 2006; Nyman et al., 2016). Other factors such as microarchitecture and past loading history, that result in accumulation of microdamage, are also material quality factors, but it is the bone tissue level material properties that play arguably the important role that underpins fragility fractures.

There are several methods for examining bone properties at the tissue level but these, of course, address slightly different aspects depending on the length scale and are doing so by different technologies.

In recent years, several publications have reported that ageing, and age-related fractures are associated with impairment of bone nanostructural mechanics. The nanoscale deformation mechanisms of bone have been proposed and largely accepted (Gupta et al., 2005) and have pushed many research groups to investigate age-related changes at the bone tissue level which could explain the increase in fracture risk. Zimmermann et al. (2011) compared cortical bone from middle aged donors and older osteoporotic donors capturing nanoscale behaviour using a combination of synchrotron X-ray diffraction and simultaneous in situ tensile testing, reporting that old bone exhibited a more pronounced plateauing of fibril strain and lower yield stress. Similarly, Ma et al. (2020) compared trabecular tissue from ageing hip-fracture donors with non-fractured controls. The data showed that fracture donors exhibited lower peak fibril and mineral strain, and tissue strain (these are strain

values at failure). Taken together these studies suggest that low mineral and fibril strain could provide a structural mechanistic origin for age-related and/or osteoporotic fragility fractures. They have also demonstrated the great value of the synchrotron-based micro/nano mechanical assessment of bone for deriving tissue level properties. Acquiring knowledge on the role of nanoscale strain in clinically relevant material properties might be useful for an improved assessment of the effects of ageing, disease, and treatment on bone and ultimately whole bone fracture risk (Abel et al., 2021).

In recent years, nanoindentation, which allows for precise measurements of local mechanical properties of bone, has been employed for in situ measurements of bone material. It is better in examining localised bone properties at the microscale and the spatial heterogeneity of cross sections of bone considering that bone microstructural features are normally from a few tens to a few hundreds of μm (Rho et al., 1997, 2002). It has also been used as a tool to determine the mechanical properties of bone, which result from the chemical quality of bone (Rho et al., 2002; Chevalier et al., 2007; Donnelly et al., 2010; Hengsberger et al., 2002) and in response to treatments (Karim et al., 2018; Schoeb, 2020). The diamond tip of the indenter interacts with bone to cause local yield by compression through a largely stable ductile loading mode which crushes bone and loads fibres by probably separating the fibril-fibril and mineral-fibril interfaces. A recent study on bovine bone which combined AFM with in-situ loading found that cracks nucleated when the fibril and fibril-mineral interfaces separated (Qian et al., 2020). Therefore, indenters could be useful for capturing the yield and microdamage structural mechanisms of bone tissue under load which precede fracture. Nanoindentation may be an alternative tool to assess bone at the tissue level for evaluating osteoporosis as well as monitor bisphosphonate (BP) treatment outcomes. However, it has been reported that the micro/nano scale values it produces for material stiffness, yield resistance and viscoelastic/plastic behaviour may not be directly comparable to mechanical properties at larger length scales (Nyman et al., 2016; Boughton et al., 2018; Gallant et al., 2013). And although it can assess bone at the tissue level independently of porosity, unless porosity and other concomitant structural features can be factored in it will be difficult to persuade clinicians and patients to adopt indentation into clinical practice.

This study used these two alternative tissue level methods on some clinically relevant material of (i) ageing non-fracture controls, (ii) ageing hip fracture patients that had been prescribed bisphosphonate therapy and (iii) untreated ageing hip fracture patients with two objectives: to elucidate the behaviour of different types of bone at the tissue level and to test the efficacy and association of the two methods by correlating and analysing the results produced by them for these three bone tissue types.

2. Materials & methods

Individuals with history of primary bone disease (except osteoporosis or osteopenia) or underlying disorders which could lead to secondary bone disease were excluded from this study. Femoral Head specimens were obtained by two centres in the UK and US as described in the ethics statement at the end and were all after informed consent had been obtained for research. In total bone from 25 individuals was employed in this study divided in three cohorts: non-fracture control (Control, N = 7, mean age = 73.29 ± 8.75), fracture untreated (Fx-Untreated, N = 10, age = 82.00 ± 5.29) and fracture treated with bisphosphonates (Fx-BisTreated, N = 8, age = 76.88 ± 8.46). Demographics by sample are shown in Table 1.

2.1. Thermogravimetric analysis

Thermogravimetric analysis and Differential Scanning Calorimetry was carried out by using a TGA/DSC 3+ (Mettler Toledo®, Indium calibrated) with a two-phase experiment (Bonicelli et al., 2022): (i)

Table 1
Demographics information for the sample divided between non-fracture control (Control), fracture (Fx-Untreated) and bisphosphonate treated fracture (Fx-BP Treated).

Donor Group	Donor Number	Sex	Age	Treatment (years)
Control	HA01	Male	84	–
	HA03	Female	73	–
	HA06	Female	82	–
	HA07	Male	73	–
	HA08	Female	72	–
	HA09	Female	72	–
	HA10	Male	57	–
Fx-Untreated	SM01	Female	82	–
	SM02	Male	79	–
	SM04	Male	91	–
	SM08	Female	90	–
	SM11	Female	76	–
	SM12	Female	84	–
	SM16	Male	79	–
	SM18	Female	75	–
	SM22	Female	82	–
	SM24	Female	82	–
Fx-BP Treated	CX09	Female	79	1
	CX57	Female	82	5
	SM03	Female	68	1
	SM05	Female	88	9
	SM09	Male	78	
	SM13	Female	79	5
	SM14	Female	61	6
	SM21	Male	80	1

dynamic temperature increase from 25 to 550 °C at a rate of 10 °C/min and (ii) a static phase in which 550 °C are kept for 10 min in order to completely eliminate the organic matrix and reduce the bone to ashes (Fig. 3). Temperature in the chamber was controlled by a continuous flow of water at room temperature. The powder was tested in air in 40 mL aluminium pans with flat bases filled with approximately 10 mg of bone powder and the weight was recorded using a microbalance (Sartorius Genius ME235), while an empty crucible was used as a reference. StarE V 16.00 was used for the curve's analysis. The bone powder for all samples was at the start relatively at the same level of dryness as samples were placed in a desiccator at room temperature for 48 h prior to testing in the DSC. The mass of 10 mg was the amount of bone that could reasonably fit in the 40 mL aluminium pans. Thermogravimetric curves (TGA) were divided in three temperature ranges and step horizontal was used to calculate percentage weight loss. Dehydration of the sample (W%, %) was calculated between ~25 and 200 °C and organic weight loss (Org%, %) between ~200 and 550 °C. The sum of the two steps represents the entire weight loss and subtracting it from 100 gives the mineral content percentage (Min%, %). The same intervals were used to calculate enthalpy values from differential scanning calorimeter curves by means of linear integration. The first endothermic episode represents the energy required to dehydrate the bone and break hydrogen bonds (LΔH, W.g^{-1}) while the second exothermic episode represents organic combustion (CΔH, W.g^{-1}).

2.2. Mechanical micro strain behaviour

Rectangular beams were prepared from all donors as per Ma et al. (2020) (Fig. 1). The ends of each specimen were potted into a 3D printed holder using dental cement (3 M™ ESPE Filtek™ Supreme XTE) which allow it to be clamped during the testing without damage or slipping. The gauge length was 6 mm and samples were stored until testing at −80 °C. The direction of the beams was practically in the radial direction and this was chosen so that the trabeculae will run along and across it but mostly in the direction of the tensile load. This was due to the fact that in the femoral head the trabeculae fan out toward the surface and show two principal directions corresponding to the direction of loading and so with appropriate care and along the radial direction one can
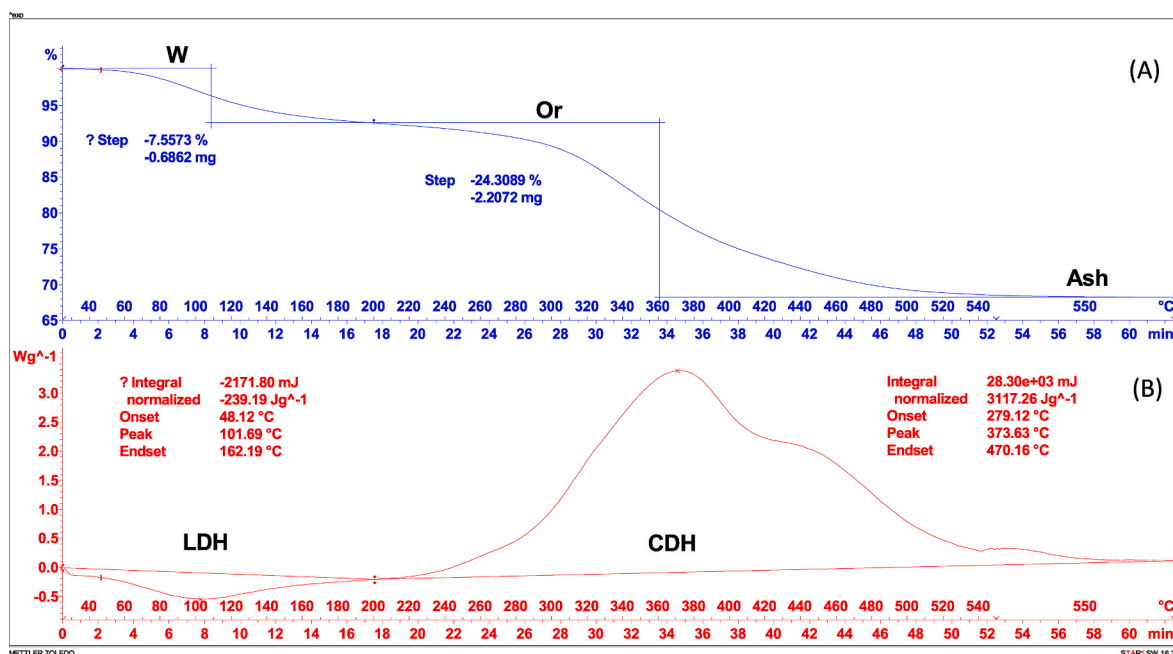
Fig. 1. Example of thermogravimetric (A) and differential scanning calorimetry (B) curves. The first weight loss represents the bone matrix dehydration and matches with the endothermic peak responsible also for triple helix thermal denaturation (LΔH). The second weight loss (Org%) represents the combustion of organic and matches with the major exothermic peak (CΔH) in the DSC curve. Subtracting from 100 the entire weight loss it is possible to obtain mineral content (Min %).

make sure it aligns the beams with the axes of symmetry of the material.

Tensile testing was carried out by means of a custom designed micromechanical rig and load cell set up and calibrated to the I22 Beamline facility settings at Diamond Light Source, UK (full details in Ma et al. (2020)). Specimens were defrosted 30 min prior to testing and kept hydrated through the experimental procedure. The testing to failure was strain controlled at a strain rate 0.001 s^{-1}. A high-speed camera was placed next to the rig to record the relative movement of two ink markers on the bone sample which were used to produce 'tissue strain' at failure via a video extensometer. Apparent stress was obtained by dividing load over the initial cross-sectional area and later normalised further (Ma et al., 2020) by dividing it by BV/TV-1.26 'Fibril strain' at failure was measured by using SAXD and measuring the stretch of the 67 nm periodicity (D) of the collagen fibres with respect to its original value. The stretching ΔD is tracked by the spacing of SAXD peaks and

hence 'fibril strain' = ΔD/D. Since the 1st order meridional peak was obscured by high-intensity mineral spectrum, the 3rd order meridional peak was considered. Furthermore, radial integration from $\pm$15° around the load direction (0°) calculated the strain in size of fibres oriented along the load direction. 'Mineral strain' at failure was calculated by using WAXD and tracking changes in length along the c-axis of the crystals using the relative stretch of the 002-diffraction peak. The sample detectors (PILATUS 2 M and RAPID) were located at 0.175 m for WAXD and 6.852 m for SAXD. Sample scanning was carried out in real-time during testing at 2.5-s intervals (X-ray exposure time of 0.5 s) at 1 Å wavelength with X-ray energy of 12.4 keV.

2.3. Nanoindentation

Nano indentation samples were prepared from the same bones as the

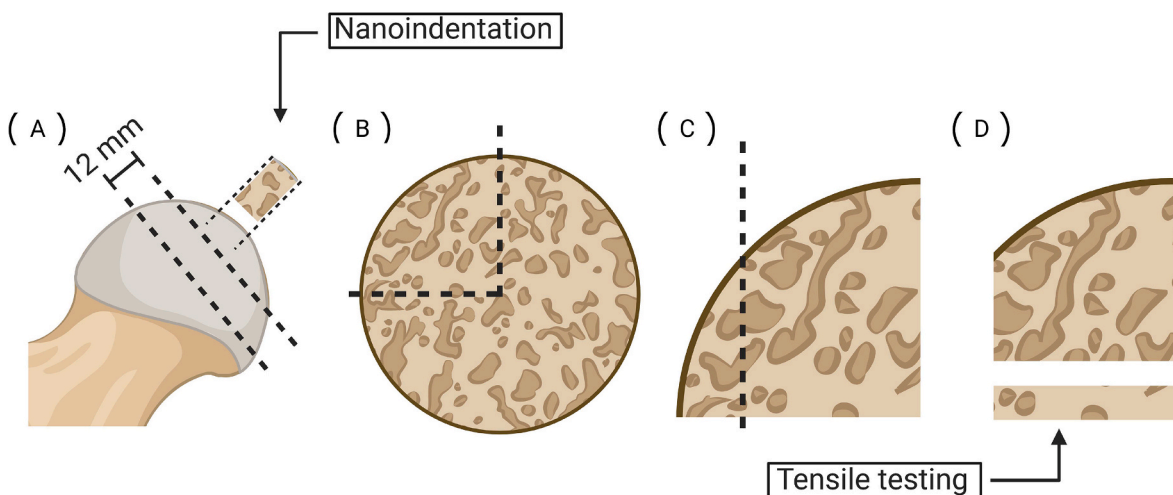**Fig. 2.** Sample preparation for STTesting. (A) 12 mm think slice of the femoral head below the fovea capitis. (B) One cut along the edge of the fovea and other at 90°. (C) Edge taken from arc facing fovea. (D) Sections cut from the end closest to the chiasma to produce the final beam for STTesting. Figure (A) also shows how the most superior distal cup section of the femoral head was used for nanoindentation cores drilling.

synchrotron tests. One centimetre wide cylindrical core samples were drilled out. A Struers Accutom wafering saw equipped with diamond impregnated blade (300 μm) was used to make a cut down the centre of each core. This produced two halves (Fig. 2), which were degreased and dried out for embedding in cold curing resin (MetPrep Kleer Set Type SSS) to expose the longitudinal and transverse cross sections according to the mediolateral axis of the femoral neck to indent trabeculae across and along their length. They were metallographically polished using an automatic Struers RotoPol-15 with 203 mm silicon carbide abrasive disks grinding paper of decreasing grit size and finally polished on a MasterTex cloth with a suspension of 0.05 mm γ-alumina slurry (Met-Prep Ltd, Coventry, UK). Testing was performed using a CSM-NHT (system v.3.75, CSM, 2034 Peseux, Switzerland) equipped with a Berkovich (triangular-based pyramid) diamond indenter. The load protocol used 10 mN maximum load hold for 30s at 20 mN/min loading/unloading rate (Bonicelli et al., 2022). Ten indentations were performed on three different transverse and three longitudinal trabeculae (these can be found in the two orthogonal planes along and across the beam) and the values from both directions were averaged.

Universal Hardness (H) was calculated from load and contact area (Equation (1)), nanoindentation modulus (E_{IT}) was obtained in the unloading phase as per Oliver and Pharr (1992) (Equation 2 a,b).

$$H = P_{max} / A \tag{1}$$

$$E_r = [\pi^{1/2} / 2\beta] [S / A^{1/2}] \tag{2a}$$

$$E^* = E_{IT} / (1-\nu_s^2) = [1/ E_r - (1-\nu_i^2) / E_i]^{-1} \tag{2b}$$

where the reduced modulus E_r is produced from the stiffness S in the retracting phase, the contact area function A and the shape factor β. The plain strain modulus E^* derives the nanoindentation modulus E_{IT} for a sample Poisson's ratio value $\nu_s = 0.3$, with elastic properties of the diamond indenter $\nu_i = 0.07$ and $E_i = 1140$ GPa. Fused silica (modulus 72 GPa, $\nu_s = 0.17$) was used to calibrate the tip shape function. Hardness was later normalised by mineral content obtained by means of TGA/DSC3+ (H/Ash). Brittleness was assessed as the ratio of hardness over elastic indentation modulus (H/E_{IT}). The energy dissipation in elastic and plastic forms has been shown to relate to the H/E ratio and hence brittleness, the reverse of toughness, can be assessed by this ratio. Indentation creep (C_{IT}) was calculated by the proportional increase in depth (Equation (3)) occurring while the load is held constant, and it represents the viscoplasticity. The indentation work ratio (η_{IT}) was obtained by examining the percentage ratio of the elastically recovered energy over the total energy input during a full indentation cycle (Equation (4))

$$C_{IT} = [(h_1-h_2)/ h_1] \times 100 \tag{3}$$

$$\eta_{IT} = [W_{elast}/ W_{elast} + W_{plast}] \times 100 \tag{4}$$

2.4. Statistical analysis

Statistical analysis was carried out in R version 4.1.1. A Shapiro-Wilk test confirmed that all variables were normally distributed. Pearson's correlation coefficient was used to evaluate interactions between strain behaviour and indentation measured mechanical properties.

3. Results

Table 2 summarises the data in descriptive statistics and the differences between groups comparing by analysis of variance in between: sex, the 3 main groups, fractured-vs-non-fractured and BP treated-vs-non-treated. Hardness was different between the 3 main groups and marginally different between fracture vs non-fracture controls. STT results were the only ones showing consistently differences between the 3 main groups and also in comparisons fracture/non-fracture and treatment/non-treatment. As for structural/quality (DSC) and composition (TGA) effects the only element that flagged out was the organic phase for 'fracture' and 'treatment' either through its quality (DSC, combustion peak CDH) or quantity (Organic%, TGA).

3.1. Patterns of behaviour

On the whole there were two patterns that emerged: one where the order of values was in rank $1 > 2 > 3$, where Control > Fx-BP Treated > Fx-Untreated (with Controls and Fractures Untreated being at the two ends of the range); and the second pattern was in the order $1 > 3 > 2$, where Control > Fx-Untreated > Fx-BP Treated (with Controls and Fractures BP treated being at the ends of the range). The parameters that followed these two patterns are shown in Table 3.

3.2. Nanoindentation

The behaviour of four nanoindentation parameters is shown in Fig. 4 C–F. Hardness (Fig. 4C) for Fx-Untreated was significantly different from both the Control and Fx-BisTreated. Comparisons of the remaining parameter did not show significant differences. In all cases it was the Fx-BisTreated which were similar to the controls and the Fx-Untreated which was the odd one out for all five nanoindentation parameters. In other words nanoindentation data appears to suggest that the residual material properties of the bone tissue of pharmacologically treated fracture victims stayed near the baseline, the baseline being the tissue properties of healthy controls.

3.3. Mechanical microstrain behaviour

Mann-Whitney test results show statistical differences for all three strain values between groups (Fig. 5A and B,C). Fibril strain was (median and range) 0.92 ± 0.46 for the non-fracture control group, 0.65 ±
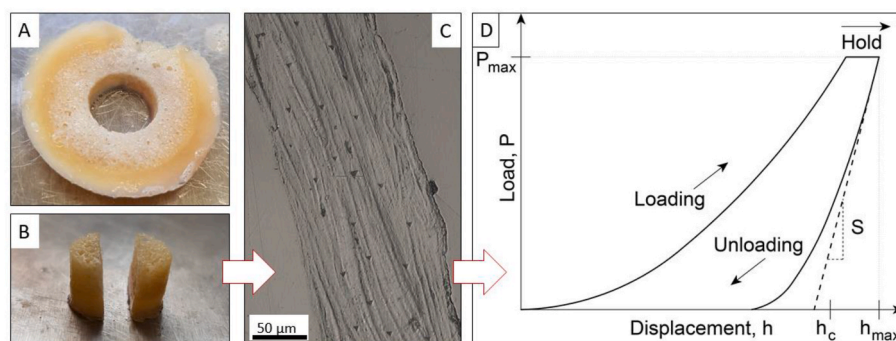

Fig. 3. Procedure to obtain tissue nanomechanical properties from the drilling of the core on the femoral head (A) that will be divided in two halves (B) in order to indent along the longitudinal and cross-section surface, (C) acquisition of the data and (D) processing of the load/depth curve.

Table 2
Descriptive statistics and ANOVA stats results for all measured parameters. Some structural and compositional parameters were different between groups.

		Sex (F/M) mean (SD)	p	3 groups (Con/FxU/FxBP) mean (SD)	p	fracture (Con/Fx) mean (SD)	p	treatment (Untr/BP) mean (SD)	p
DSC	**LDHOnset (C)**	**72.9 (4.3)** **68.6 (4.3)**	**0.030****	73.2 (4.0) 71.1 (4.5) 70.5 (5.6)	0.516	73.2 (4.0) 70.8 (4.8)	0.260	72.0 (4.3) 70.5 (5.6)	0.463
	LDHpeak (C)	101.3 (4.0) 98.9 (5.2)	0.229	100.7 (5.2) 101.1 (3.1) 99.8 (5.6)	0.838	100.7 (5.2) 100.5 (4.3)	0.922	100.9 (4.0) 99.8 (5.6)	0.563
	LDH-E (W/g)	119.4 (8.6) 113.4 (6.3)	0.096*	120.5 (7.5) 113.8 (7.0) 119.3 (9.6)	0.206	120.5 (7.5) 116.3 (8.5)	0.261	116.6 (7.8) 119.3 (9.6)	0.462
	CDHOnset (C)	318.4 (2.9) 320.7 (4.4)	0.146	319.17 (4.1) 318.93 (4.1) 319.40 (2.8)	0.965	319.17 (4.1) 319.14 (3.5)	0.985	319.03 (3.9) 319.40 (2.8)	0.815
	CDHpeak (C)	385.5 (12.2) 389.1 (16.3)	0.540	392.9 (16.2) 388.1 (13.3) 379.4 (7.9)	0.138	392.8 (16.2) 384.2 (11.2)	0.152	390.0 (14.3) 379.4 (7.9)	0.062*
	CDH-E (W/g)	**3275 (227)** **3615 (204)**	**0.001****	3543 (251) 3333 (274) 3315 (257)	0.188	3543 (251) 3323 (257)	0.065*	3409 (272) 3333 (274)	0.523
TGA	**Organic (%)**	**26.8 (0.71)** **28.1 (1.35)**	**0.006****	27.8 (1.06) 27.4 (1.17) 26.7 (0.86)	0.141	27.8 (1.06) 27.1 (1.06)	0.116	27.5 (1.12) 26.7 (0.86)	0.079*
	Mineral (%)	64.9 (0.92) 64.0 (2.31)	0.175	64.2 (1.06) 64.8 (1.61) 64.8 (1.81)	0.649	64.2 (1.06) 64.8 (1.65)	0.348	64.6 (1.42) 64.8 (1.81)	0.725
	Min/Org	**2.417 (0.086)** **2.285 (0.189)**	**0.023****	2.310 (0.1250) 2.377 (0.1478) 2.430 (0.1303)	0.254	2.310 (0.1250) 2.400 (0.1388)	0.145	2.350 (0.1390) 2.430 (0.1303)	0.180
Nano-indentation	**Hardness (MPa)**	372.7 (36) 357.4 (23)	0.284	**349.5 (29)** **387.7 (32)** **358.9 (26)**	**0.031****	349.5 (29) 374.9 (32)	0.081*	371.9 (36) 358.9 (25)	0.363
	Elastic Modulus (GPa)	13.0 (0.8) 12.8 (0.4)	0.408	12.8 (0.7) 13.3 (0.7) 12.7 (0.7)	0.190	12.8 (0.7) 13.0 (0.8)	0.429	13.1 (0.7) 12.7 (0.8)	0.263
	Brittleness	28.6 (2.1) 28.0 (1.8)	0.500	27.4 (1.9) 29.3 (2.1) 28.3 (1.6)	0.175	27.4 (1.9) 28.8 (1.9)	0.117	28.6 (2.2) 28.3 (1.6)	0.816
	Creep (%)	5.182 (0.340) 5.286 (0.276)	0.459	5.410 (0.352) 5.100 (0.191) 5.192 (0.374)	0.142	5.410 (0.352) 5.141 (0.282)	0.058*	5.227 (0.303) 5.192 (0.374)	0.794
	Indentation Work	28.9 (1.37) 28.6 (1.82)	0.700	28.2 (1.52) 29.2 (1.35) 29.0 (1.67)	0.412	28.2 (1.52) 29.1 (1.46)	0.187	28.7 (1.46) 29.0 (1.67)	0.746
STT - Micro strains	**Tissue Strain (%)**	0.936 (0.3192) 1.184 (0.4044)	0.175	**1.340 (0.3208)** **0.990 (0.1181)** **0.663 (0.0563)**	**<0.001****	**1.340 (0.3208)** **0.814 (0.1901)**	**<0.001****	**1.178 (0.3005)** **0.663 (0.0563)**	**<0.001****
	Fibril Strain (%)	0.583 (0.2443) 0.765 (0.2307)	0.160	**0.885 (0.1763)** **0.634 (0.0746)** **0.368 (0.0623)**	**<0.001****	**0.885 (0.1763)** **0.491 (0.1524)**	**<0.001****	**0.769 (0.1868)** **0.368 (0.0623)**	**<0.001****
	Mineral Strain (%)	0.113 (0.03996) 0.148 (0.04589)	0.119	**0.165 (0.03009)** **0.124 (0.01705)** **0.076 (0.00704)**	**<0.001****	**0.165 (0.03009)** **0.099 (0.02863)**	**<0.001****	**0.147 (0.03153)** **0.076 (0.00704)**	**<0.001****

$P < 0.01$ *.
$P < 0.05$ **.

0.21 for the Fx-Untreated; significantly lower for the Fx-BisTreated at 0.36 ± 0.21. Control and Fx-BisTreated cohorts were statistically different from Fx-BisTreated. Fx-BisTreated values for mineral strain (Fig. 5C) were significantly lower compared to the remaining two groups and the same pattern was present for tissue strain in Fig. 5A.

3.4. Thermal analysis, composition and matrix quality

The enthalpy of the organic phase combustion (CDH-E, collagen quality) produced by DSC correlated with the Organic content % (collagen quantity) produced by TGA ($R = 0.739$; $P < 0.001$) as seen in Fig. 6. As expected mineral and organic contents related significantly ($R = -0.778$; $P < 0.001$) an outcome of the in-situ maturation phase of bone tissue where mineral substitutes for organic, resulting in them increasing and decreasing their contents respectively.

In composition, no significant difference across the three groups were found for mineral, or organic content. The Control group showed lower degree of mineralisation compared to the two fractured groups, but these differences were not statistically significant at $P = 0.05$. It is also interesting that in the two fracture cohorts, mineral content levels seem to be almost identical. In contrast, organic content shows the lowest values for the Fx-BP Treated group with the organic content values being in the rank order 1- Control/2- Fx-Untreated/3- Fx-BP Treated, similar to the order of values we observed for the STT mechanical micro-strain behaviour tests.

Table 3

Nanoindentation data and enthalpy parameters LDH-E, CDH-E showed an order of rank: *Control > Fx-BP Treated > Fx-Untreated*, while the STT mechanical data, the rest of the DSC data and the composition values (Organic%, Mineral/Organic ration and Water%) showed an order of rank: *Control > Fx-Untreated > Fx-BP Treated*.

|	Control > Fx-BP Treated > Fx-Untreated	Control > Fx-Untreated > Fx-BP Treated
	1 > 2 > 3	1 > 3 > 2
DSC (structural)	LDH-E	LDHonset
	CDH-E	LDHpeak
		CDHonset
		CDHpeak
TGA (composition)		Organic %
		Mineral/Organic ratio
Mechanical characterisation	Hardness (Nano)	Tissue strain (STT)
	Indentation Modulus (Nano)	Fibril strain (STT)
	Brittleness (Nano)	Mineral strain (STT)
	Creep (Nano)	
	Elastic Work ratio (Nano)	

3.5. Mechanical correlations

The mechanical test results (primarily STT) exhibited some relation to both DSC (qualitative) and TGA (composition, quantitative) structural data. Nanoindentation hardness had a weak correlation (P = 0.074 < 0.1) to CDH-E (combustion of the organic phase), while STT data related (P < 0.050) to CDHpeak and CDH-E and to composition (Organic %, Water % and Mineral/Organic ratio). The intercorrelation between the two types of mechanical behaviour was significant for *indentation work ratio* -vs- mineral strain (P < 0.05), but weak for tissue (P = 0.055) and fibril strain (P = 0.061). These are summarised in Table 4 and shown in Figs. 7 and 8. An important observation was that the STT strains were related to the Organic content, the Mineral/Organic ratio and the Water content, but not to the Mineral content itself. This possibly signifies a qualitative difference between the influence of each of the 3 moieties of bone tissue (mineral, organic, water) on the STT microstrain behaviour.

4. Discussion

The aim of this study was to test the association between nano-mechanical material strain behaviour and indentation measured
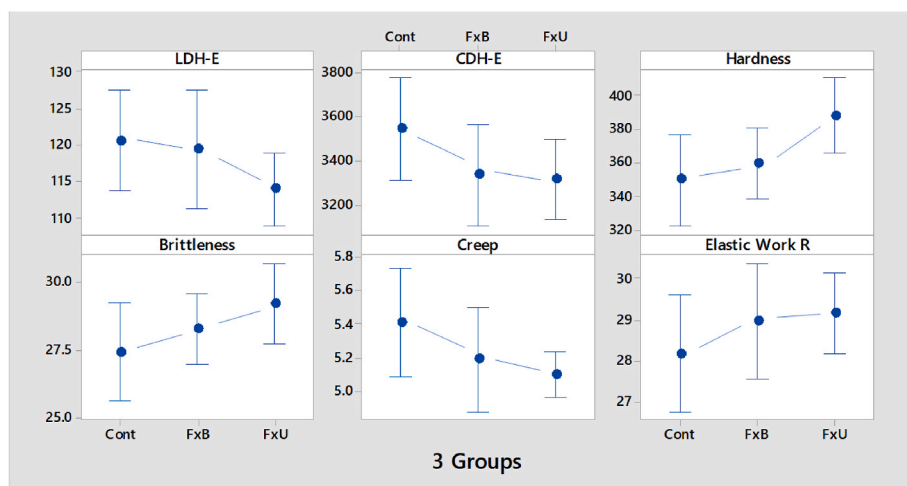
Fig. 4. Relative behaviour of the 3 groups in nanoindentation and two structural (LDH-E, CDH-E) parameters (A, B). Nanoindentation testing (C–F) reveals that Fx-Un treated tissue properties were further apart from Control (healthy) group than the Fx BP treated group. (* Mann-Whitney P < 0.05).
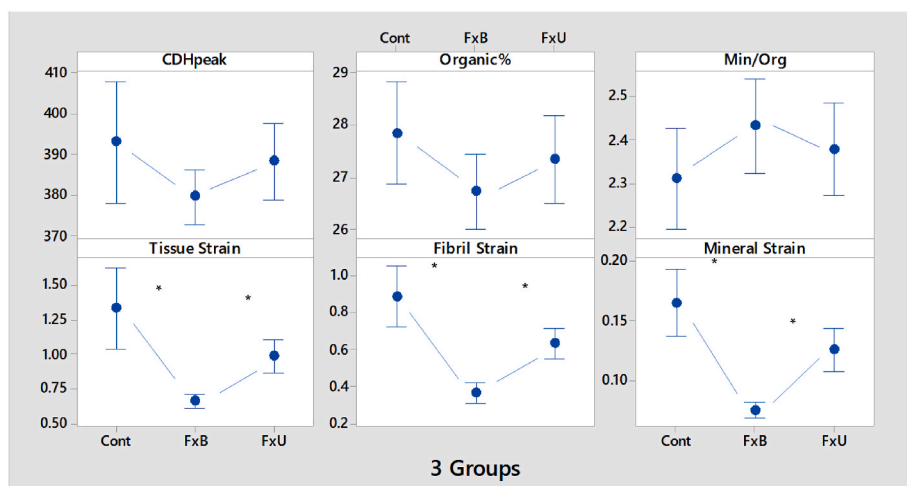
Fig. 5. Controls reach significantly greater strains (fibril, mineral and tissue strain) at failure than fracture patients, irrespective of treatment. Relative ranking of the STT strains behaviour across the three main groups. Organic content, Mineral to Organic ratio (from TGA) and some of the structural parameters (from DSC) behave in a similar manner to the STT behaviour. (* Mann-Whitney P < 0.05).
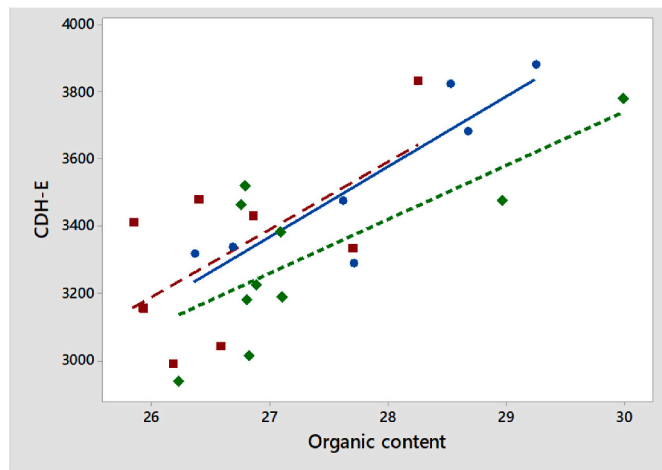
Fig. 6. The enthalpy for combustion of the organic phase (measured by DSC) was related to the organic content (measured by TGA), and this dependency was the same (statistically non-different) for all three types of tissue (Blue-controls, Red-fracture BP treated; Green-fracture untreated).

Table 4
STT and nanoindentation parameters relating to some DSC and TGA data.

Mechanical parameter	Structural parameter	Pearson's correlation coefficient	Level of significance P
Hardness (MPa)	**CDH-E (W/g)**	−0.364	0.074
Tissue Strain (%)	**CDH peak (Cº)**	0.566	**0.009***
Fibril Strain (%)	**CDH peak (Cº)**	0.542	**0.013***
Mineral Strain (%)	**CDH-E (Cº)**	0.517	**0.019***
Tissue Strain (%)	**CDH-E (W/g)**	0.534	**0.015***
Fibril Strain (%)	**CDH-E (W/g)**	0.494	**0.027***
Mineral Strain (%)	**CDH peak (W/g)**	0.516	**0.020***
Tissue Strain (%)	**Organic (%)**	0.623	**0.003***
Fibril Strain (%)	**Organic (%)**	0.586	**0.007***
Mineral Strain (%)	**Organic (%)**	0.615	**0.004***
Tissue Strain (%)	**Mineral/Organic**	−0.530	**0.016***
Fibril Strain (%)	**Mineral/Organic**	−0.496	**0.026***
Mineral Strain (%)	**Mineral/Organic**	−0.513	**0.021***
Tissue Strain (%)	**Water (%)**	−0.547	**0.013***
Fibril Strain (%)	**Water (%)**	−0.531	**0.016***
Mineral Strain (%)	**Water (%)**	−0.592	**0.006***
Tissue Strain (%)	**Indentation Work ratio**	−0.435	0.055
Fibril Strain (%)	**Indentation Work ratio**	−0.425	0.061
Mineral Strain (%)	**Indentation Work ratio**	−.0444	**0.050***

mechanical properties using clinically relevant bone tissue samples from the proximal femora of three ageing donor groups. Results showed that 1- the *Control* group exhibited the highest values of fibril, mineral and tissue strain at failure, followed by 2- the *Fx-Untreated* and last 3- the *Fx-BP Treated*. These particular differences were strongly associated with a similar variation pattern seen for organic content, suggesting a functional relationship between organic content and mechanical strain behaviour. In contrast, nanoindentation hardness values showed a rank order of: 1- Control followed by 2- Fx-BP Treated and lastly 3- Fx-Untreated. The same tendency, although not significant was shown by nanoindentation elastic modulus. No clear correlations were found between compositional and nanoindentation mechanical properties. Irrespective of treatment, hip-fractures were associated with low material strain at tissue and nano level in comparison to controls. This shows that the mechanistic basis for what is exhibited at a higher length scale derives from the potency of the material at the nano level. Specifically, low strain in the collagen-mineral building blocks may provide a structural mechanistic origin for low strains at the tissue level. It is hard to argue that low strain does not contribute to fracture exactly because by reducing the material ability to absorb energy the resistance to cracking and fracturing is reducing. In contrast, the indentation mechanical properties of the Controls were more similar to Fx-BisTreated donors than Fx-Untreated, indicating that therapy might have some restorative effect. The caveat of course is that calling this rank order of properties 'restorative' is relative to the judgement passed that whatever returns the tissue to a condition nearest to controls is desirable and optimal. This is questionable because it is the measured property that is being 'restored' which returns to the former state not the material itself. Consequently, the results of the present study demonstrate the importance of studying mechanical properties of mineralised collagen fibres using multiple investigation tools, each of which may illuminate different aspects of material behaviour.

4.1. Mineral or organic?

STT strains correlated to the amount of organic, the mineral/organic ratio, the water content, but not to the mineral content itself. Knowing that with the addition of mineral this element substitutes for water (the tissue becomes drier) the correlation with water content and the lack of correlation with mineral content shows that the fracture behaviour does not depend on the amount of the mineral per se, but on the condition (hydration level) and amount of its complimentary phase the organic content. Mineral content clearly had no effect on any of the three STT strains. It has been reported (Zioupos et al., 1994; Currey, 2004) that the accumulation of microdamage due to strain failure initiation is not dependent on the degree of mineralisation and it starts at ~5500 microstrain for tissues from various species with greatly different mineral contents. The present study also indicates that it is the collagen that plays a central role in fracture resistance. This concept is also supported by the Acevedo et al. (2015) study which proposed the hypothesis that strain supported by collagen fibrils is compromised by the treatment due to post-translational matrix modifications rather than modifications in the mineral phase (Saito et al., 2008; Allen et al., 2008). The two phases mineral and collagen are complementary to each other, so we may conclude that the impaired energy dissipation and fragility of over mineralised BP treated bone is not cause by the mineral content itself but by the concomitant reduction in organic content.

4.2. Hip fractures associated with low strain

Tensile testing with simultaneous measurements of strain showed that, fracture patients are characterised by lower deformation capability at both micro- and nano-mechanical level. The present results showed lower values for tissue, mineral and fibril strain for bisphosphonate treated trabecular specimens compared to both controls and untreated fracture patients and disagree with Zimmermann et al. (2016) who
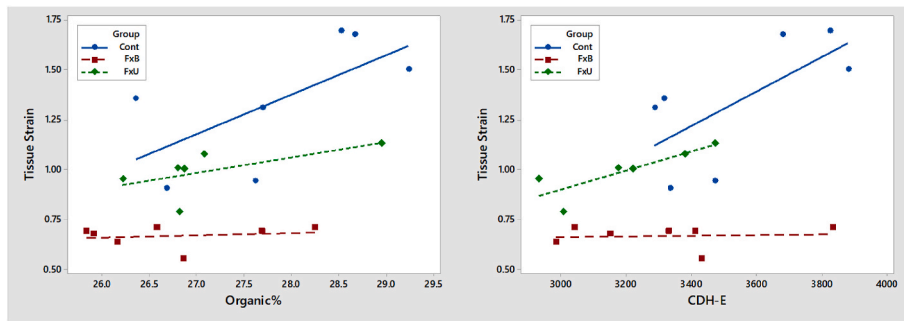
Fig. 7. STT tissue strain (one of the 3 strains measured, chosen as an example for this illustration and because bone fracture is evidenced at the tissue level) -vs- organic content % and CDH-E. The two fracture groups show lower tissue strains a strong indicator that fragility in-vivo is linked to impaired deformation capability and here shown to be associated with the quantity and quality of the organic content too. The most severe effects on tissue strain are for the fracture-BP treated group where the bone was most fragile despite being pharmacologically treated with BP. (Blue-controls; Green-fracture untreated; Red-fracture BP treated).
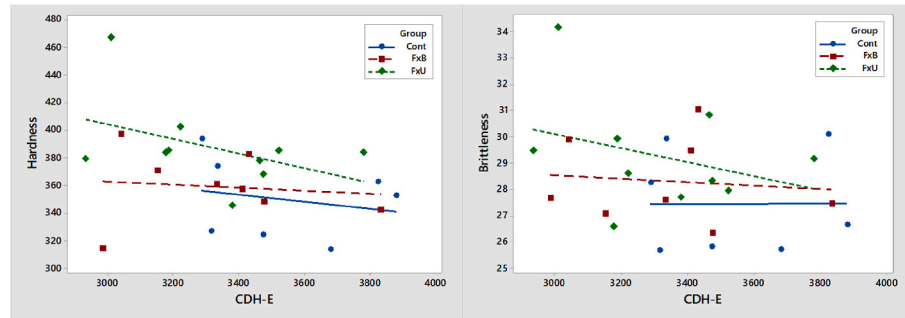
Fig. 8. Nanoindentation hardness and brittleness -vs- CDH-E. The control group shows lower brittleness and hardness than the fracture groups. These patterns are not statistically significant (slopes, intercepts or group differences) due to the noise and variability of the data. (Blue-controls; Green-fracture untreated; Red-fracture BP treated).

reported a beneficial effect of BP treatment in strain behaviour, although crucially these researchers were working on cortical tissue instead. The present results in cancellous samples show as much as 31% lower maximum fibril strain between a healthy control and fractured group, while Zimmermann et al. (2016) in cortical specimens found a 40% lower fibril strain in fracture tissue compared to the controls. Bone mechanical integrity has been strongly associated with physicochemical composition and architecture of its components, fashioned in its unique three-dimensional hierarchical organisation. The balance between the mineral, organic and water components is essential in keeping the accumulation of damage at a low level and preventing fracture (Burr, 2019; Jin et al., 2017; Zioupos, 2001). The accumulation of micro-damage, not evaluated in the present study, and the consequent impaired performance is also associated with age-related changes of collagen and mineral (Boskey and Imbert, 2017). These physiological modifications are predominant in older age individuals when bone conditions are normally aggravated by impaired turnover and metabolic conditions (Ma et al., 2020; Acevedo et al., 2015; Zimmermann et al., 2016).

Impaired bone turnover caused by normal physiological ageing with metabolic disorder and bisphosphonate treatment has also been suggested to induce modifications of the organic matrix such as accumulation of non-enzymatic cross-links, decrease collagen quality and non-collagenous proteins (Zimmermann et al., 2016). Present results show that the fracture cohorts regardless of treatment had lower collagen content compared to Controls (Ma et al., 2017, 2020; Acevedo et al., 2015; Zimmermann et al., 2016). However, the effect of bisphosphonates treatment on posttranslational collagen modification (collagen quality) has not been unanimously accepted and the effect of treatment intensity and duration have been seen to heavily affect bone matrix changes in several different ways (Saito et al., 2008; Gourion-Arsiquaud et al., 2010; Saito and Marumo, 2010). Ma et al. (2020) suggested that the reduction in mechanical properties in relation with long term bisphosphonate treatment could be due not only to the binding action of the drug on the mineral which suppresses bone remodelling, but also

may induce posttranslational modification of the collagen component (Saito et al., 2008), exacerbating the age-related matrix degeneration and resulting in increased fragility.

4.3. Bisphosphonates therapy associated with restored indentation measured properties

Indentation measured nanohardness is considerably greater in the Controls and Fx-BisTreated than Fx-Untreated. The four other indentation parameters do not vary significantly across the three groups although the trends are similar and with larger sample size perhaps significant. Higher values in hardness and stiffness in the fracture group were also associated with higher values in the brittleness parameter which is hardness normalised by indentation modulus. Although both modulus and hardness increased in this group, their ratio, which is taken as indicative of brittleness, was still higher than both Controls and Fx-BisTreated. It would be sensible to assume that this brittleness derives from an increased mineralisation of collagen fibres (Fratzl-Zelman et al., 2009). Several published studies have reported an increase in hardness and elastic modulus and mineral content with advanced age and bisphosphonate treatments and with increased association to fragility fractures, however this does not in itself establish a cause/effect relationship between these factors. BP treatments are more likely to affect mineral crystal growth indirectly by controlling the turnover rate and thus raising the average mineral content and prolonging the in-situ age of the crystals (crystals not dissolved are ageing in-situ). This, however, does not seem to contribute directly and unequivocally to understanding bone fracture behaviour and therefore nanoindentation might not represent ideal avenue for understanding increase in fragility in relation with age (Nyman et al., 2016; Lloyd et al., 2017; Pienkowski et al., 2019).

Restoration of indentation measured mechanical properties, particularly hardness, most likely is a by-product of the basic action of these drugs which bind the surface of mineral crystals, reducing dissolution and proliferation. It has been reported that bisphosphonates increase

mineral content, but there is not clear agreement as to how crystal size changes with bisphosphonate therapy (Boskey, 2003; Eanes and Hailer, 2000). A reduction in crystal size has been reported for by osteoporotic iliac crest biopsies (Durchschlag et al., 2006). Previous studies have shown that increased mineral content results in higher indentation modulus and hardness that could explain higher results for the Fx-Untreated group (Zioupos, 2005). Furthermore, low modulus and hardness values are normally attributed to small crystal size (Rho et al., 2001; Vanleene et al., 2012; Wen et al., 2015).

4.4. Evaluating fragility and assessing treatment outcomes

Nanostrain and indentation measured mechanical properties exhibit different patterns of variation between groups, and the two data sets are not correlated. Thus, it seems that they vary independently. Hence nano indenters do not seem to capture nanomechanical behaviour or the structural mechanisms that lead to damage formation. The lack of association between synchrotron tensile test nanostrains and nano-indentation data might point to a difference in their utility value for assessing bone health. The only relationship we found suggests that a decrease in viscoplastic behaviour (increase in elastic/plastic indentation work ratio) of mineralised collagen fibres has a negative effect on strain behaviour. This was previously identified as a contributing factor in increased bone fragility (Wu et al., 2012). The relationship could suggest that strain behaviour changes resulting from long-term term BP treatment could be primarily related to modifications of collagenous matrix.

Overall, tissue, mineral and fibrils nanostrain at failure were lower in fractured patients, regardless of treatment status. This data supports the conclusion that reduced peak fibril and mineral strain are associated with reduced bone deformability in patients with age-related hip-fractures. As a result, analysis of strain behaviour at the nanostructural level is a valid approach to evaluate risk of fracture and it could have important clinical applications (Abel et al., 2021). In contrast, indentation measured mechanical properties did not distinguish between BP treated fracture victims and controls. One could argue that BP had restored the properties of the bone material, but this is only true for properties expressed by the nano-indentation characterisation method. Nanoindentation has been shown to be a valuable method to examine mechanical properties in spatially heterogeneous bone sections comprising bone packets of variable mineral contents, loading history and tissue age (Rho et al., 2002; Zioupos et al., 2008), but in the present context did not seem to be informative regarding bone strength and fracture risk of drug treated bone material. In this study, STT nanostrains at tissue, fibril and mineral level were more reliable for predicting fragility at the macro-tissue level. There may be some cross-over effects between mineralisation profile of the three groups, modifications at various structural levels and chemistry which need to be deconvoluted to decipher the combined effects of all these structural and micromechanical alterations. This must be done by examining them in parallel and from the same samples to exclude cross-correlations and thus identify those that are principal causes of fragility in ageing -vs- BP treatment (Zioupos, 2001). The present study would be more reliable with a larger sample size and the effects of bisphosphonate could be better assessed with the inclusion of an unfractured bisphosphonate treatment cohort too. The cross-sectional nature of study design does not reveal variation in the mechanical properties of the tissues during treatment (longitudinal aspect). Lastly, we have examined bone tissue samples from the cancellous regions of the femoral head because fragility fractures occur predominantly in calculous rich bone regions. It would have been good to test cortical regions in parallel to cancellous from these same samples, a topic for future work.

5. Conclusions

The propensity of bone to fracture depends on its properties at

different structural levels and length scales. In the present study we used two material characterisation techniques: nanoindentation and tensile tests under synchrotron radiation which were able to monitor strains at the mineral and organic level by use of SAXS and WAXS. Composition (mineral and collagen contents) was assessed by thermogravimetric analysis and was related to the bone tissue properties and strain behaviour. Tissue from three cohorts of volunteers was examined (i) healthy controls (ii) untreated fracture patients and (iii) BP treated fracture patients. It is difficult to grade objectively these 3 groups in terms of the quality and performance of the bone tissue. However, working from the premise that the 'worst' tissue is the one that despite the BP treatment sustained fractures, we can conclude that tracking the mechanical behaviour of the fibril, mineral and tissue strains is a reliable way of assessing bone fragility because in this respect the Fx-BP treated group came out worst of the three. Nanoindentation and composition showed that despite the common conception that fracture can be prevented by increasing mineral density in bone tissue, this cannot simply be mineral content alone because this is associated with increased fragility. Collagen content on the other hand appeared to relate to bone behaviour, with healthy controls having a higher organic content and achieving higher fibril, mineral and tissue strains. The fact that mineral content alone worked against fragility could open new avenues in the explanation of age-related fractures and potential treatment, because BP have been proven to induce an increment in bone mineral per unit volume and this may bring about the wrong effect. Despite the preliminary nature of this study, it is obvious that bone fragility goes beyond bone mass, mineral density and content and warrants further research on the biophysical and chemical aspects of the two bone moieties the collagen and mineral. In order to define the unique composite properties of bone its properties at different structural levels and length scales have to be understood and assessed to enable us to address strength and risk of fracture successfully.

Ethics

Ethical approval was granted by the Imperial College Tissue Bank (R13004) and samples were collected in accordance with the ethical standards of the institutional and national research committees and with the 1964 Helsinki Declaration and its later amendments. Femora from non-fracture donors came from cadavers donated to the Biological Resource Centre (AZ, USA) and permission to research the tissue was granted by the donor or next of kin. Fracture bone samples were collected from patients with an intracapsular fracture in the neck of femur after written informed consent was provided at St Mary's Hospital (London, United Kingdom) between May 2016 and September 2017.

CRediT authorship contribution statement

Andrea Bonicelli: Writing – original draft, Methodology, Investigation. **Tabitha Tay:** Project administration, Methodology, Data curation, Conceptualization. **Justin P. Cobb:** Funding acquisition, Conceptualization. **Oliver R. Boughton:** Methodology, Funding acquisition, Conceptualization. **Ulrich Hansen:** Investigation, Funding acquisition, Conceptualization. **Richard L. Abel:** Resources, Investigation, Funding acquisition, Conceptualization. **Peter Zioupos:** Writing – review & editing, Writing – original draft, Supervision, Resources, Project administration, Methodology, Investigation, Funding acquisition, Formal analysis, Data curation, Conceptualization.

Declaration of competing interest

The authors declare that they have no known competing financial interests or personal relationships that could have appeared to influence the work reported in this paper.

Data availability

Data underlying this paper can be accessed at CORD (Cranfield Online Research Data) https://cranfield.figshare.com

References

Abel, R.L., Stavri, R., Gray, M., Hansen, U., 2021. Clinical importance of bone matrix damage mechanisms for fracture prevention. Curr. Osteoporos. Rep. https://doi.org/10.1007/s11914-021-00678-8.

Acevedo, C., Bale, H., Gludovatz, B., Wat, A., Tang, S.Y., Wang, M., Busse, B., Zimmermann, E.A., Schaible, E., Allen, M.R., Burr, D.B., Ritchie, R.O., 2015. Alendronate treatment alters bone tissues at multiple structural levels in healthy canine cortical bone. Bone 81, 352–363. https://doi.org/10.1016/j.bone.2015.08.002.

Allen, M.R., Gineyts, E., Leeming, D.J., Burr, D.B., Delmas, P.D., 2008. Bisphosphonates alter trabecular bone collagen cross-linking and isomerization in beagle dog vertebra. Osteoporos. Int. 19 (3), 329–337. https://doi.org/10.1007/s00198-007-0533-7.

Bonicelli, A., Kranioti, E.F., Xhemali, B., Arnold, E., Zioupos, P., 2022. Assessing bone maturity: compositional and mechanical properties of rib cortical bone at different ages. Bone 155, 116265. https://doi.org/10.1016/j.bone.2021.116265.

Boskey, A., 2003. Bone mineral crystal size. Osteoporos. Int. 14, 16–21. https://doi.org/10.1007/s00198-003-1468-2.

Boskey, A.L., Imbert, L., 2017. Bone quality changes associated with aging and disease: a review. Ann. N. Y. Acad. Sci. 1410, 93–106. https://doi.org/10.1111/nyas.13572.

Boughton, O.R., Ma, S., Zhao, S., Arnold, M., Lewis, A., Hansen, U., Cobb, J.P., Giuliani, F., Abel, R.L., 2018. Measuring bone stiffness using spherical indentation. PLoS One 12 (7), e0200475. https://doi.org/10.1371/journal.pone.0200475, 13.

Burr, D.B., 2019. Changes in bone matrix properties with aging. Bone 120, 85–93. https://doi.org/10.1016/j.bone.2018.10.010.

Chevalier, Y., Pahr, D., Allmer, H., et al., 2007. Validation of a voxel-based FE method for prediction of the uniaxial apparent modulus of human trabecular bone using macroscopic mechanical tests and nanoindentation. J. Biomech. 40, 3333–3340. https://doi.org/10.1016/j.jbiomech.2007.05.004.

Currey, J.D., 2004. Tensile yield in compact bone is determined by strain, post-yield behaviour by mineral content. J. Biomech. 37 (4), 549–556. https://doi.org/10.1016/j.jbiomech.2003.08.008.

Donnelly, E., Boskey, A.L., Baker, S.P., Van Der Meulen, M.C.H., 2010. Effects of tissue age on bone tissue material composition and nanomechanical properties in the rat cortex. J. Biomed. Mater. Res. 92, 1048–1056. https://doi.org/10.1002/jbm.a.32442.

Durchschlag, E., Paschalis, E.P., Zoehrer, R., Roschger, P., Fratzl, P., Recker, R., Phipps, R., Klaushofer, K., 2006. Bone material properties in trabecular bone from human iliac crest biopsies after 3- and 5-year treatment with risedronate. J. Bone Miner. Res. 21, 1581–1590. https://doi.org/10.1359/jbmr.060701.

Eanes, E.D., Hailer, A.W., 2000. Anionic effects on the size and shape of apatite crystals grown from physiological solutions. Calcif. Tissue Int. 66, 449–455. https://doi.org/10.1007/s002230010090.

Fratzl-Zelman, N., Roschger, P., Gourrier, A., Weber, M., Misof, B.M., Loveridge, N., Reeve, J., Klaushofer, K., Fratzl, P., 2009. Combination of nanoindentation and quantitative backscattered electron imaging revealed altered bone material properties associated with femoral neck fragility. Calcif. Tissue Int. 85, 335–343. https://doi.org/10.1007/s00223-009-9289-8.

Gallant, M.A., Brown, D.M., Organ, J.M., Allen, M./R., David B Burr, D.B., 2013. Reference-point indentation correlates with bone toughness assessed using whole-bone traditional mechanical testing. Bone 53 (1), 301–305. https://doi.org/10.1016/j.bone.2012.12.015.

Gourion-Arsiquaud, S., Allen, M.R., Burr, D.B., Vashishth, D., Tang, S.Y., Boskey, A.L., 2010. Bisphosphonate treatment modifies canine bone mineral and matrix properties and their heterogeneity. Bone 46, 666–672. https://doi.org/10.1016/j.bone.2009.11.011.

Gupta, H.S., Wagermaier, W., Zickler, G.A., Aroush, R.-B.D., Funari, S.S., Roschger, P., Wagner, H.D., Fratzl, P., 2005. Nanoscale deformation mechanisms in bone. Nano Lett. 5, 2108–2111. https://doi.org/10.1021/nl051584b.

Hengsberger, S., Kulik, A., Zysset, P., 2002. In: Nanoindentation Discriminates the Elastic Properties of Individual Human Bone Lamellae under Dry and Physiological

Conditions, vol. 30, pp. 178–184. https://doi.org/10.1016/s8756-3282(01)00624-x, 1.

Jin, A., Cobb, J., Hansen, U., Bhattacharya, R., Reinhard, C., Vo, N., Atwood, R., Li, J., Karunaratne, A., Wiles, C., Abel, R., 2017. The effect of long-term bisphosphonate therapy on trabecular bone strength and microcrack density. Bone and Joint Research 6, 602–609. https://doi.org/10.1302/2046-3758.610.BJR-2016-0321.R1.

Karim, L., Vliet, M. Van, Bouxsein, M.L., 2018. Comparison of cyclic and impact-based reference point indentation measurements in human cadaveric tibia. Bone 106, 90–95. https://doi.org/10.1016/j.bone.2015.03.021.

Larrue, A., Rattner, A., Peter, Z.A., Olivier, C., Laroche, N., Vico, L., Peyrin, F., 2011. Synchrotron radiation micro-CT at the Micrometer scale for the analysis of the three-dimensional morphology of microcracks in human trabecular bone. PLoS One 6. https://doi.org/10.1371/journal.pone.0021297.

Lloyd, A.A., Gludovatz, B., Riedel, C., Luengo, E.A., Saiyed, R., Marty, E., 2017. Atypical fracture with long-term bisphosphonate therapy is associated with altered cortical composition and reduced fracture resistance. Proc. Natl. Acad. Sci. USA 114, 8722–8727. https://doi.org/10.1073/pnas.1704460114.

Ma, S., Goh, E.L., Jin, A., Bhattacharya, R., Boughton, O.R., Patel, B., Karunaratne, A., Vo, N.T., Atwood, R., Cobb, J.P., Hansen, U., Abel, R.L., 2017. Long-term effects of bisphosphonate therapy: perforations, microcracks and mechanical properties. Sci. Rep. 7, 1–10. https://doi.org/10.1038/srep43399.

Ma, S., Goh, E.L., Tay, T., Wiles, C.C., Boughton, O., Churchwell, J.H., Wu, Y., Karunaratne, A., Bhattacharya, R., Terrill, N., Cobb, J.P., Hansen, U., Abel, R.L., 2020. Nanoscale mechanisms in age-related hip-fractures. Sci. Rep. 10, 1–14. https://doi.org/10.1038/s41598-020-69783-5.

Nyman, J.S., Granke, M., Singleton, R.C., Pharr, G.M., 2016. Tissue-level mechanical properties of bone contributing to fracture risk. Curr. Osteoporos. Rep. 14, 138–150. https://doi.org/10.1007/s11914-016-0314-3.

Oliver, W.C., Pharr, G.M., 1992. An improved technique for determining hardness and elastic modulus using load and displacement sensing indentation experiments. J. Mater. Res. 7, 1564–1583. https://doi.org/10.1557/JMR.1992.1564.

Pienkowski, D., Wood, C.L., Malluche, H.H., 2019. Young's modulus and hardness of human trabecular bone with bisphosphonate treatment durations up to 20 years. Osteoporos. Int. 30, 277–285. https://doi.org/10.1007/s00198-018-4760-x.

Qian, T., Chen, X., Hang, F., 2020. Journal of the Mechanical Behavior of Biomedical Materials Investigation of nanoscale failure behaviour of cortical bone under stress by AFM. J. Mech. Behav. Biomed. Mater. 112, 103989 https://doi.org/10.1016/j.jmbbm.2020.103989.

Rho, J.Y., Tsui, T.Y., Pharr, G.M., 1997. Elastic properties of human cortical and trabecular lamellar bone measured by nanoindentation. Biomaterials 18, 1325–1330. https://doi.org/10.1016/S0142-9612(97)00073-2.

Rho, J.Y., Mishra, S.R., Chung, K., Bai, J., Pharr, G.M., 2001. Relationship between ultrastructure and the nanoindentation properties of intramuscular herring bones. Ann. Biomed. Eng. 29, 1082–1088. https://doi.org/10.1114/1.1424913.

Rho, J.Y., Zioupos, P., Currey, J.D., Pharr, G.M., 2002. Microstructural elasticity and regional heterogeneity in human femoral bone of various ages examined by nano-indentation. J. Biomech. 35, 189–198. https://doi.org/10.1016/S0021-9290(01)00199-3.

Saito, M., Marumo, K., 2010. Collagen cross-links as a determinant of bone quality: a possible explanation for bone fragility in aging, osteoporosis, and diabetes mellitus. Osteoporos. Int. 21, 195–214. https://doi.org/10.1007/s00198-009-1066-z.

Saito, M., Mori, S., Mashiba, T., Komotsubara, S., Marumo, K., 2008. Collagen maturity, glycation induced-pentosidine, and mineralization are increased following 3-year treatment with incadronate in dogs. Osteoporosis and Sarcopenia 19, 1343–1354. https://doi.org/10.1007/s00198-008-0585-3.

Schoeb, M., 2020. Treatments of Osteoporosis Increase Bone Material Strength Index in Patients with Low Bone Mass 1683-1690. https://doi.org/10.1007/s00198-020-05375-3.

Seeman, E., Delmas, P.D., 2006. Bone quality - the material and structural basis of bone strength and fragility. N. Engl. J. Med. 354, 2250–2261. https://doi.org/10.1056/nejmra053077.

Vanleene, M., Porter, A., Guillot, P.V., Boyde, A., Oyen, M., Shefelbine, S., 2012. Ultra-structural defects cause low bone matrix stiffness despite high mineralization in osteogenesis imperfecta mice. Bone 50, 1317–1323. https://doi.org/10.1016/j.bone.2012.03.007.

Wen, X.X., Wang, F.Q., Xu, C., Wu, Z.X., Zhang, Y., Feng, Y.F., Yan, Y.B., Lei, W., 2015. Time related changes of mineral and collagen and their roles in cortical bone mechanics of ovariectomized rabbits. PLoS One 10, 1–18. https://doi.org/10.1371/journal.pone.0127973.

Wu, Z., Ovaert, T.C., Niebur, G.L., 2012. Viscoelastic properties of human cortical bone tissue depend on gender and elastic modulus. J. Orthop. Res. 30, 693–699. https://doi.org/10.1002/jor.22001.

Zimmermann, E.A., Schaible, E., Bale, H., Barth, H.D., Tang, S.Y., Reichert, P., Busse, B., Alliston, T., Ager, J.W., Ritchie, R.O., 2011. Age-related changes in the plasticity and toughness of human cortical bone at multiple length scales. Proc. Natl. Acad. Sci. U. S. A. 108, 14416–14421. https://doi.org/10.1073/pnas.1107966108.

Zimmermann, E.A., Schaible, E., Gludovatz, B., Schmidt, F.N., Riedel, C., Krause, M., Vettorazzi, E., Acevedo, C., Hahn, M., Püschel, K., Tang, S., Amling, M., Ritchie, R. O., Busse, B., 2016. Intrinsic mechanical behavior of femoral cortical bone in young, osteoporotic and bisphosphonate- treated individuals in low- and high energy fracture conditions. Sci. Rep. 6, 1–12. https://doi.org/10.1038/srep21072.

Zioupos, P., 2001. Ageing human bone: factors affecting its biomechanical properties and the role of collagen. J. Biomater. Appl. 15, 187–229. https://doi.org/10.1106/5JUJ-TFJ3-JVVA-3RJ0.

Zioupos, P., 2005. In vivo fatigue microcracks in human bone: material properties of the surrounding bone matrix. Eur. J. Morphol. 42, 31–41. https://doi.org/10.1080/09243860500095463.

Zioupos, P., Currey, J.D., Sedman, A.J., 1994. An examination of the micromechanics of failure of bone and antler by acoustic emission tests and Laser Scanning Confocal Microscopy. Med. Eng. Phys. 16, 203–212. https://doi.org/10.1016/1350-4533(94)90039-6.

Zioupos, P., Gresle, M., Winwood, K., 2008. Fatigue strength of human cortical bone: age, physical, and material heterogeneity effects. J. Biomed. Mater. Res. 86, 627–636. https://doi.org/10.1002/jbm.a.31576.